Role of alkali-resistant glassfiber in suppression of restrained shrinkage cracking of concrete materials

Chote Soranakom, Mehdi Bakhshi, Barzin Mobasher
Arizona State University, Tempe, USA

Summary

The role of alkali-resistant (AR)-glassfiber in improving the cracking resistance of concrete subjected to drying shrinkage is studied by experimental and analytical approaches. The experiments utilize the ring-type restrained shrinkage test and monitor strain history in the steel ring as concrete is exposed to an arid environment. Results of control and alkali-resistant glassfiber-reinforced concrete (AR-GFRC) specimens indicate that glassfiber slightly delays the time of cracking but drastically minimizes crack widths. A systematic methodology based on an image analysis approach is used to measure crack width growth in a concrete ring specimen. An analytical approach that relates key influential parameters including diffusion, shrinkage, creep, aging material properties and restraining effect is presented. The theoretical model was used to calibrate and interpret the experimental test results, providing a better understanding of how a drying environment generates tensile stresses and crack widening in the restrained concrete specimens. The theoretical model for predicting steel strain history and concrete crack width in a restrained shrinkage test shows good correlation with the experimental data.

1. Introduction

In hot and low-humidity environments, concrete shrinks due to loss of moisture from the capillary and gel pore microstructure. It is also well known that the tensile strength of concrete at early age is very low. When concrete is cast in place and restrained from free shrinkage, tensile stress develops and may crack if the stress exceeds the material strength. The extent of shrinkage is determined by many factors, including mix proportions, relative humidity, temperature and geometry of the structure [1].

One possible method to reduce the adverse effect of cracking is the addition of short glassfibers; however, there is a paucity of quantitative methods for assessing the ability of fibers to resist cracks in concrete. A restrained shrinkage test configuration referred to as AASHTO PP34-99 [2] has been recently adopted to measure the susceptibility of concrete mixtures to cracking. This procedure is similar to other restrained tests developed by other researchers [1]. Various theoretical approaches for modelling the restrained shrinkage cracking of concrete have been developed [3]. These models try to address the interaction between material properties and the shrinkage characteristics of concrete.

Meanwhile, there is no model to properly predict the post-cracking behaviour of plain concrete and AR-GFRC in the restrained shrinkage test. The simulation of crack width opening, which is of great importance, is also lacking. In this paper a model for predicting restrained shrinkage behavior before and after cracking is presented and calibrated with the experimental data. This model is capable of showing the effects of adding fiber on the restrained shrinkage and cracking of concrete.

2. Theoretical modelling of restraint shrinkage

In order to model the mechanism of the ring-type restrained shrinkage test, an analytical approach was developed based on a previous model by Mane *et al.* [4]. The model incorporates essential aspects of diffusion in concrete, free shrinkage, creep behaviour, strength characteristic of aging materials and restraining effect of the steel ring. The proposed algorithm allows continuous monitoring of stress and strain developed in a concrete specimen.

2.1. Moisture diffusion and free shrinkage

As concrete loses its moisture to the environment and free shrinkage takes place, the humidity profile *h(z)* through the thickness of the concrete section is simplified using Fick's law of diffusion:

$$h(z) = h_s - (h_s - h_i)erf(z) \qquad (1)$$

where *z* is the distance measured from the outside surface inwards of the specimen, h_s and h_i represent the humidity (fraction) at the outside surface and interior section and *erf(z)* represents the error function [5]. A cubic function is used to relate the free shrinkage strain as a function of the humidity profile throughout the thickness.

$$\varepsilon_{sh\infty}(z) = \varepsilon_{sh\infty}(1 - h(z)^3) \qquad (2)$$

where $_{sh\infty}$ is the free drying shrinkage strain at infinite time, which can be obtained from the empirical relationship proposed by Bazant and Panula [6]. The time-dependent shrinkage is assumed to follow the empirical form suggested by the ACI [7]:

$$\varepsilon_{sh}(z,t) = \frac{t^{\xi}}{f + t^{\xi}} \varepsilon_{sh\infty} \qquad (3)$$

where *f* and are constants and *t* is time in days.

2.2. Creep of concrete

As concrete is subjected to tensile stress, it produces creep strain with time to offset the strain due to free shrinkage, resulting in relaxation of the elastic stresses in the material. Due to the lack of an early-age tensile creep model, it is assumed that the creep coefficient of concrete in compression $v(t)$ used in the ACI code [7] is applicable to the present tensile mode of loading.

$$v(t) = \frac{t^{\psi}}{d + t^{\psi}} v_u \qquad (4)$$

where v_u is the ultimate creep coefficient, *d* and are constants and *t* is time in days.

2.3. Age-dependent concrete strength

To estimate the properties of concrete, empirical relationships are presented as a function of concrete strength at 28 days, f_{c28}. The ACI building code [7] suggests the relationship for determining concrete compressive strength at any ages $f_c(t)$ as:

$$f_c(t) = \frac{t}{a + bt} f_{c28} \qquad (5)$$

where *t* is time in days, and *a* and *b* are constants that depend on the type of concrete and curing method. Due to a lack of tensile strength parameters at early age of concrete, it is assumed that the tensile strength of concrete, $f_t(t)$, Young's modulus $E_c(t)$, and fracture energy $G_f(t)$ increase with a square root proportional to the gain in compressive strength defined as:

$$f_t(t) = f_{t28}\sqrt{\frac{f_c(t)}{f_{c28}}} \quad E_c(t) = E_{c28}\sqrt{\frac{f_c(t)}{f_{c28}}} \quad G_f(t) = G_{f28}\sqrt{\frac{f_c(t)}{f_{c28}}} \qquad (6)$$

where f_{t28}, E_{c28} and G_{f28} are tensile strength, Young's modulus and fracture energy of concrete at 28 days, respectivey. As an alternative to the assumed time-dependent material properties, the parameters at several ages in the expected range of restrained shrinkage can be obtained from testing and established empirical relationship for the mixes considered. The tensile stress strain–crack width model for any age as shown in Fig. 1 can be constructed from the parameters defined in equation (6). The proposed model uses the stress–strain approach for both pre- and post-peak responses. Crack width derived from fracture energy is converted to strain by dividing it by the circumferential length of a concrete ring specimen.

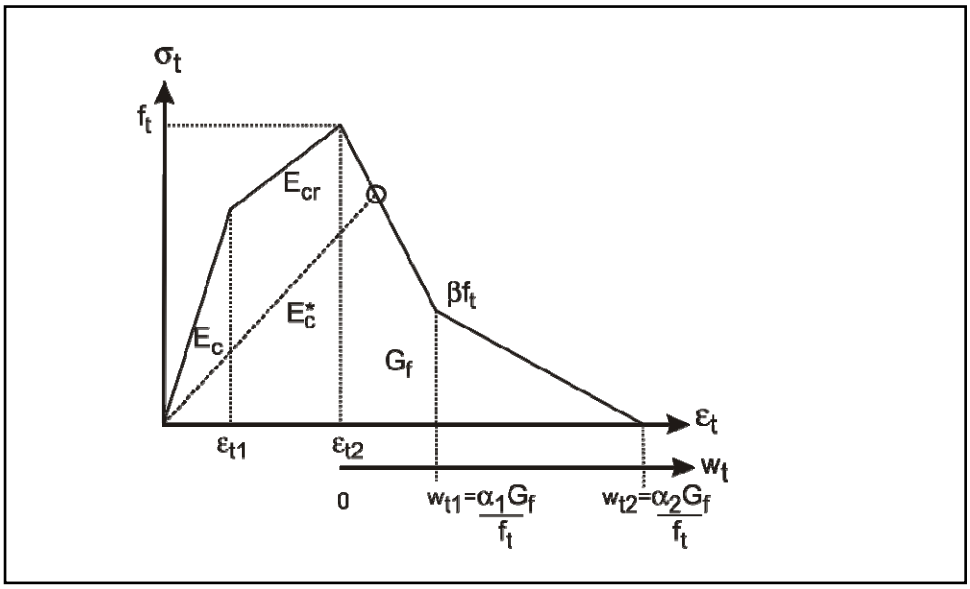

Fig. 1. Concrete tensile stress–strain and crack width model

2.4. Restraining effect of steel ring

The following sign convention and notation are used. Tensile strain is positive while compressive and shrinkage strains are negative. Forces and stresses follow the same sign as strains. Symbol is used for the incremental change of quantities between previous time step t_{j-1} and the current time step t_j; index i is used for the layer number at particular location z_i measured from the top surface of the specimen. The restraining effect provided by the steel ring that prohibits concrete from shrinking freely can be determined by equilibrium of forces between the tension force in concrete F_c (positive) and compression force in steel (negative) F_{st}.

$$\Delta F_c + \Delta F_{st} = 0 \qquad (7)$$

In the equilibrium, only the elastic tensile strain component of the concrete $_{el}$ produces stress and it is balanced with the compressive stress in steel, which has elastic compressive strain $_{st}$. Using modulus of materials, the equilibrium of force in equation (9) can be written as:

$$\Delta\varepsilon_{el}\overline{E_c^*}(t_{j-1})A_c + \Delta\varepsilon_{st}E_sA_s = 0 \qquad (8)$$

where $\overline{E_c^*}(t_{j-1})$ is the secant modulus of the concrete at previous time step averaged from all discretized concrete layers. This is only an approximation since the modulus at the current time step is not yet known. E_s is Young's modulus of steel; A_c and A_s are area of concrete and steel, respectively. By rearranging the terms in equation (8), the incremental compressive steel strain $_{st}$ is obtained as:

$$\Delta\varepsilon_{st} = -\frac{\overline{E_c^*}(t_{j-1})A_c}{E_sA_s}\Delta\varepsilon_{el} \qquad (9)$$

2.5. Stress–strain development

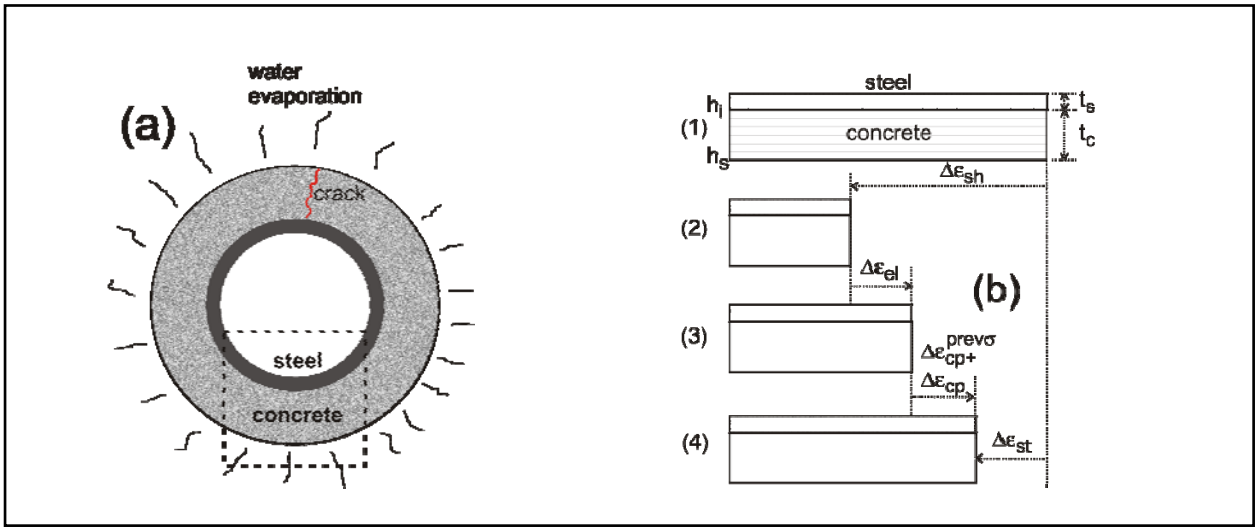

Fig. 2. Schematic drawing for drying shrinkage model: (a) ring specimen; (b) strain components

Figure 2(a) shows a concrete ring specimen subjected to moisture loss until it cracks. An arch segment of the ring as shown in the insert can be approximated to a 1D problem as depicted in Fig. 2(b); the curvature is assumed to be sufficiently small. The figure represents a schematic drawing of strain components developed in the concrete ring specimen. The free shrinkage strain $_{sh}$ (negative) will be restrained by the steel ring, creating compressive strain in the steel $_{st}$ (negative), and the steel compressive force must be balanced with the tension force in the concrete, which immediately generates elastic strain in the concrete $_{el}$ (positive). For time interval t, the concrete tensile stress will generate creep strain $_{cp}$ (positive). In addition, the previous stress history before time t_{j-1} also contributes to the creep strain increment between time t_{j-1} and t_j, $\Delta\varepsilon_{cp}^{(prev\sigma)}$, which can be calculated by using Boltzmann's superposition principle:

$$\Delta\varepsilon_{cp}^{(prev\sigma)} = \left\{ \sum_{k=2}^{j-1} \left| \frac{1}{2} \frac{\sigma_{el_k} - \sigma_{el_{k-1}}}{E_{c28}} \right| v(t_j - t_{k-1}) \right\} - \varepsilon_{cp}(t_{j-1}) \qquad (10)$$

Therefore, the equilibrium of incremental strains developed between time step t_{j-1} and t_j can be written as:

$$-\Delta\varepsilon_{sh} = \Delta\varepsilon_{el} + \Delta\varepsilon_{cp} + \Delta\varepsilon_{cp}^{(prev\sigma)} - \Delta\varepsilon_{st} \qquad (11)$$

By integrating the restraining steel strain $_{st}$ from equation (9) into equation (11), this yields

$$-\Delta\varepsilon_{sh} = \frac{\overline{E_c^*}(t_{j-1})A_c}{E_s A_s}\Delta\varepsilon_{el} + \Delta\varepsilon_{el} + \Delta\varepsilon_{cp} + \Delta\varepsilon_{cp}^{(prev\sigma)} \qquad (12)$$

By using the relationship between tensile stress and creep coefficient $_{cp} = {}_{el}C(dt)/E_{c28}$ to determine creep strain, and integrating into equation (12) this yields:

$$-\Delta\varepsilon_{sh} = \frac{\overline{E_c^*}(t_{j-1})A_c + E_s A_s}{E_s A_s}\Delta\varepsilon_{el} + \Delta\sigma_{el}\frac{v(dt)}{E_{c28}} + \Delta\varepsilon_{cp}^{(prev\sigma)} \qquad (13)$$

To obtain stress and strain distribution, concrete thickness is discretized into N_c sub-layers while steel has only one layer. The incremental elastic stress in layer i located at z_i can be expressed as:

$$\Delta\sigma_{el}(z_i) = [\varepsilon_{el}(z_i, t_j) - \varepsilon_{el}(z_i, t_{j-1})]E_c^*(z_i, t_{j-1}) = \Delta\varepsilon_{el}(z_i)E_c^*(z_i, t_{j-1}) \qquad (14)$$

After integrating incremental stress $_{el}(z_i)$ defined in equation (14) into equation (13) and rearranging the terms, the incremental concrete elastic strain at each sub-layer can be expressed as:

$$\Delta\varepsilon_{el}(z_i) = \frac{-\Delta\varepsilon_{sh}(z_i) - \Delta\varepsilon_{cp}^{(prev\sigma)}(z_i)}{Q + \dfrac{E_c^*(z_i, t_{j-1})}{E_{c28}}v(dt)}; \quad Q = \frac{\overline{E_c^*}(t_{j-1})A_c + E_s A_s}{E_s A_s} \qquad (15)$$

It should be noted that the concrete is considered as a whole thickness with an average secant modulus $\overline{E_c^*}(t_{j-1})$ in accounting for the restraining effect from steel, while concrete is treated individually with its secant modulus at each layer $E_c^*(z_i, t_{j-1})$ for the effect of free shrinkage and creep.

2.6. Algorithm for strain history in steel ring and crack width at concrete surface

(1) Calculate free shrinkage strain distribution at each layer *i* from equation (3) and its increment by:

$$\Delta\varepsilon_{sh}(z_i) = \varepsilon_{sh}(z_i, t_j) - \varepsilon_{sh}(z_i, t_{j-1}) \qquad (16)$$

(2) Calculate incremental elastic tensile strain at each layer due to free shrinkage, restraining effect and creep from equation (15).

(3) Update total elastic strain, stress and secant modulus using the concrete model described in Fig. 1.

$$\varepsilon_t(z_i, t_j) = \varepsilon_t(z_i, t_{j-1}) + \Delta\varepsilon_{el}(z_i) \qquad (17)$$

$$\sigma_t(z_i, t_j) = function[\varepsilon_t(z_i, t_j)] \ \ from\ Fig.1 \qquad (18)$$

$$E_c^*(z_i, t_j) = \frac{\sigma_t(z_i, t_j)}{\varepsilon_t(z_i, t_j)} \qquad (19)$$

(4) If the updated strain $_t(z_i, t_j)$ exceeds the strain at peak stress $_{t2}(t_j)$, the crack width at each layer of concrete is calculated by:

$$w_t(z_i, t_j) = \left[\varepsilon_t(z_i, t_j) - \varepsilon_{t\_unload}(z_i, t_j)\right]\pi D(z_i) \qquad (20)$$

where $_{t,unload}(z_i, t_j)$ is the unloading strain in the pre-peak stress–strain curve corresponding to the same stress level as the strain in the post-peak response $_t(z_i, t_j)$ and $D(z_i)$ is the diameter of the concrete ring at location z_i.

(5) Sum concrete force at each concrete layer A_{ci} to obtain the total tensile force, where the magnitude equals the compressive the force in steel.

$$F_c(t_j) = \sum_{i=1}^{N_C} A_{ci}\sigma_t(z_i, t_j) \ \text{ and } \ F_s(t_j) = -F_c(t_j) \qquad (21)$$

(6) Calculate nominal stress and strain in steel, defined by:

$$\sigma_{ns}(t_j) = \frac{F_s(t_j)}{A_s}; \ \ \varepsilon_{ns}(t_j) = \frac{\sigma_{ns}(t_j)}{E_s} \qquad (22)$$

(7) A complete strain history of the steel ring and crack width at the concrete surface can be obtained by repeating steps (1)–(6) until the time t_j reaches the specified age.

3. Experimental program

The effect of adding AR-glassfibre to normal-strength concrete was studied by restrained shrinkage test. Both plain concrete (control) and AR-glassfiber concrete (AR-GFRC) mixes were used. Commercially available high-performance (HP) AR-glassfibre obtained from VETROTEX, Cem-FIL SAINT-GOBAIN was used in this experiment. Type II Portland cement was used in all mixtures and the water/cement (w/c) ratio was 0.55. The cement content of both mixtures was 680 kg/m^3 and the slump ranged between 50 and 65 mm (2–2.5 in.). Table 1 presents the proportions of the concrete mixes.

Mix	AR-GFRC	Control
Portland cement	680	680
Fine aggregates	1360	1360
Water	374	374
Glassfibre (HP)	5	0.0
w/c	0.55	0.55
Sand/cement	2.0	2.0

Table 1. Mix proportions of the AR-GFRC and control samples (kg/m³)

An instrumented ring test similar to the AASHTO specification PP34-99 was performed to quantify the restrained shrinkage and tensile creep behavior of the concrete. The specimen consisted of a 66.675 mm (2.625 in.) thick annulus of concrete cast around a rigid steel ring 11.2 mm (0.5 in.) thick with a diameter of 289.56 mm (11.4 in.) and a height of 133.35 mm (5.25 in.). The top surface of the concrete specimen was sealed to allow drying to occur only from the outer circumferential surface of the concrete specimen. Since the height of the specimen (5.25 in.) was twice its thickness (2.625 in.), it is assumed that uniform shrinkage took place along the height of specimen.

The strain in the steel ring was measured with strain gages, while the crack widths were measured at two different ages using a high-resolution digital camera and implementing a systematic procedure of image analysis. Two strain gauges were mounted on the inside surface of the steel ring at mid-height and 90°apart. Each strain gauge was connected to the interface module using another dummy temperature compensating gauge in the form a half-bridge. The response from the strain gauges was collected by an SCXI-1321(16-channel, half-bridge) module, SCXI-1000 carrier and NI data acquisition device and transferred to a PC. A LABVEIW program previously developed was used to measure the strain gauge readings recorded at one-minute intervals.

3.1. Test procedure

Two concrete ring specimens were cast for each mixture. The specimens were demolded after 24 hours of moist-curing under plastic sheets and the top surface of the ring specimens were sealed before placing in the shrinkage chamber for strain monitoring. As shown in Fig. 3, the environmental chamber containing two racks was used for placing four specimens with two specimens at each level. The relative humidity within the chamber was maintained at 30 ± 1% RH and the specimens were exposed to drying at 40 ± 1°C (104 ± 2°F). Steel strain measurements were recorded from one day after casting, with subsequent measurements taken every minute, until two to three weeks after the concrete cracked. The strain in the steel ring was calculated as the mean value of two measured strains mounted on each sample.

Fig. 3. Experimental set-up of shrinkage test and recording of strain gauge readings

3.2. Image analysis procedure

In order to measure the crack width, an image analysis approach was adopted in this study. Imaging was performed for all specimens after 14 days' and 21 days' drying in the chamber. The samples were mounted on a rotating round plate and a digital camera (Pulnix TM1325CL) was used to take pictures. This set-up is able to scan the entire surface of the specimen and examine for new cracks and the measurements of the widths of already existing cracks. Images were acquired along the crack length using a series of eight to twelve images. The reconstruction of images accounted for the overlap during the analysis phase by intentionally cutting off the overlapping portion of the images. As illustrated in Fig. 4, the binary image (black and white) obtained from the grey-scale image using a MATLAB code was used for crack measurement.

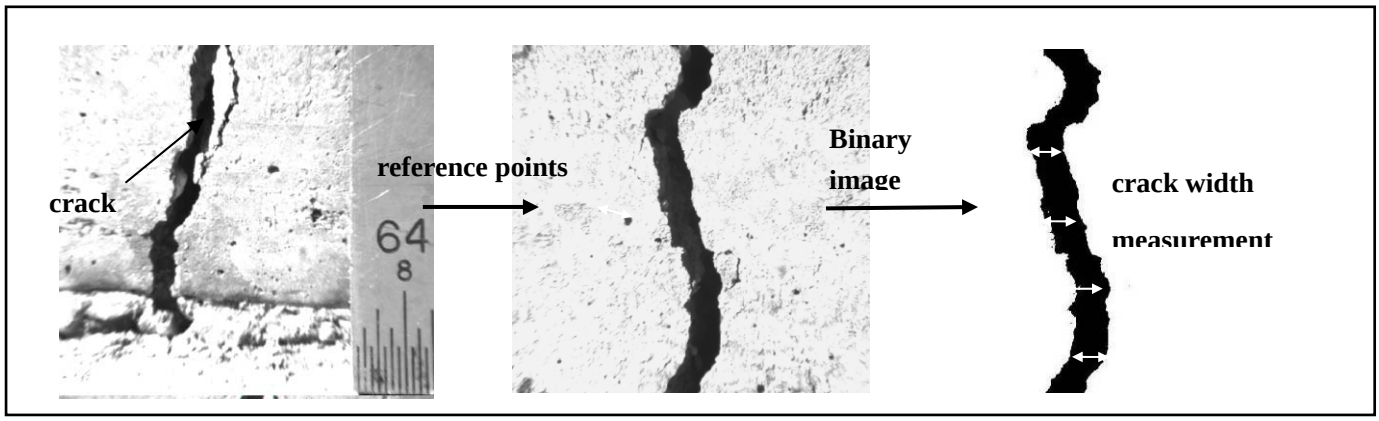

Fig. 4. Image analysis process

4. Test results, model calibration and discussion

The strain in the steel ring due to drying shrinkage strain for both the control and the AR-GFRC samples is shown in Fig. 5. The time at cracking was 3.5 and 4.5 days after curing for the control and AR-GFRC specimens, respectively. The maximum steel ring strain for the control mixes at the time of cracking was slightly lower than the values for the corresponding AR-GFRC mixes. Meanwhile the measured strains of control samples after cracking are approximately zero, showing that the concrete completely lost its ability to transfer the forces, while the AR-GFRC samples show some significant strains in the post-crack zone. Due to the random distribution of fibers in AR-GFRC, the measured strains of the samples have a greater deviation than the control samples. The average crack width of control samples after 14 days was 1.15 mm (0.0454 in.) with standard deviation of 0.0787 mm (0.0031 in.); and for AR-GFRC, it was 0.341 mm (0.01341 in.) with standard deviation of 0.048 mm (0.0019 in.). After 21 days, the average crack widths of the control and AR-GFRC samples were 1.44 mm and 0.42 mm (0.0567 in. and 0.0166 in.) respectively with standard deviations of 0.124 mm (0.0049 in.) for the control and 0.422 mm (0.0166 in.) for the AR-GFRC. The results indicate a significant difference (up to three times less) when crack width dimensions in the AR-GFRC and control specimens are compared.

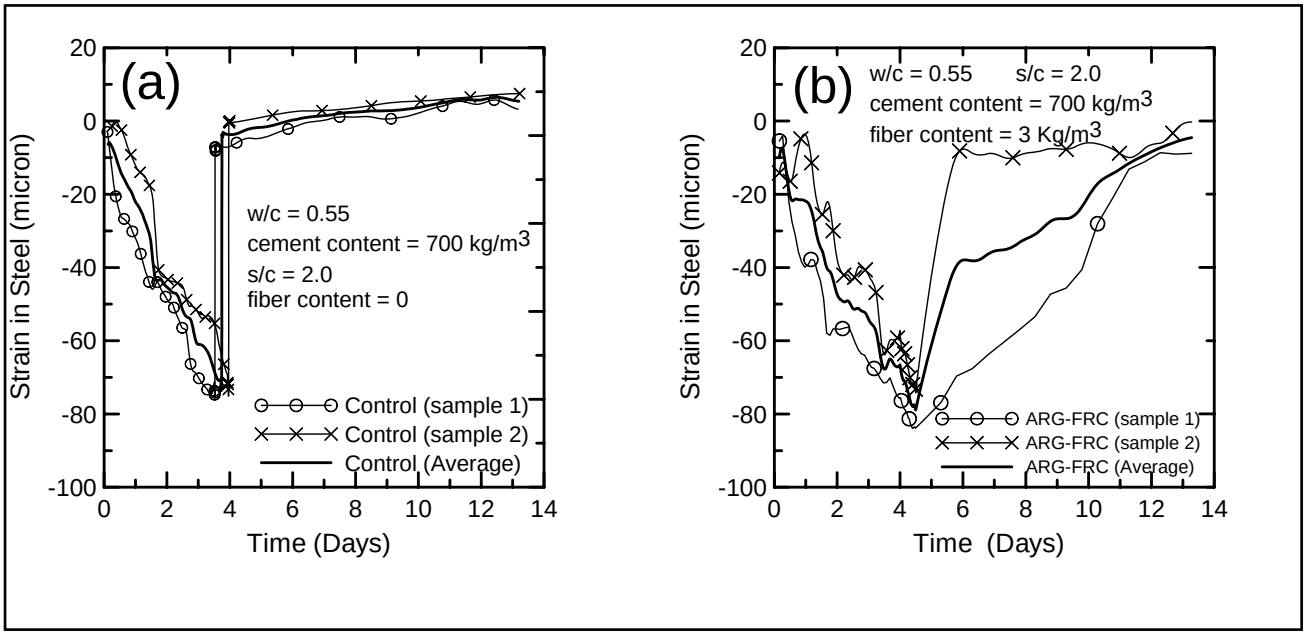

Fig. 5 Steel ring strain versus time for: (a) control; and (b) AR-GFRC specimens

The strain gage history and measured crack widths were also used to calibrate the theoretical model. The input functions for the control and AR-GFRC mixes including free shrinkage at the outer surface, creep coefficients, concrete compressive strength development and tensile stress–strain relationship were calculated by the model. The model predictions for these functions based on the coefficients described in section 2 are presented in Fig. 6(a–d). In this simulation, the ultimate shrinkage strain for AR-GFRC is assumed to be 25% less than the control mix and the creep coefficient is assumed to be twice that of the control at 28 days in order for the model to fit the experimental results. For compressive strength modelling of both the AR-GFRC and control mixes, the same strength of 28 MPa (4000 psi) at 28 days is considered. The assumed tensile stress–strain response models show the same tensile strength for both the AR-GFRC and control mixes. Meanwhile, as shown in Fig. 6(d), based on the chosen value for G_f, much more energy is dissipated in the AR-GFRC compared to the plain concrete in the post-peak zone. Based on these inputs, the theoretical simulation can fit the experimental data. Fig. 7(a) shows the steel strain prediction and Fig. 7(b) presents the crack width model for both the control and AR-GFRC samples. The model shows good correlation with the experimental results of both mixtures.

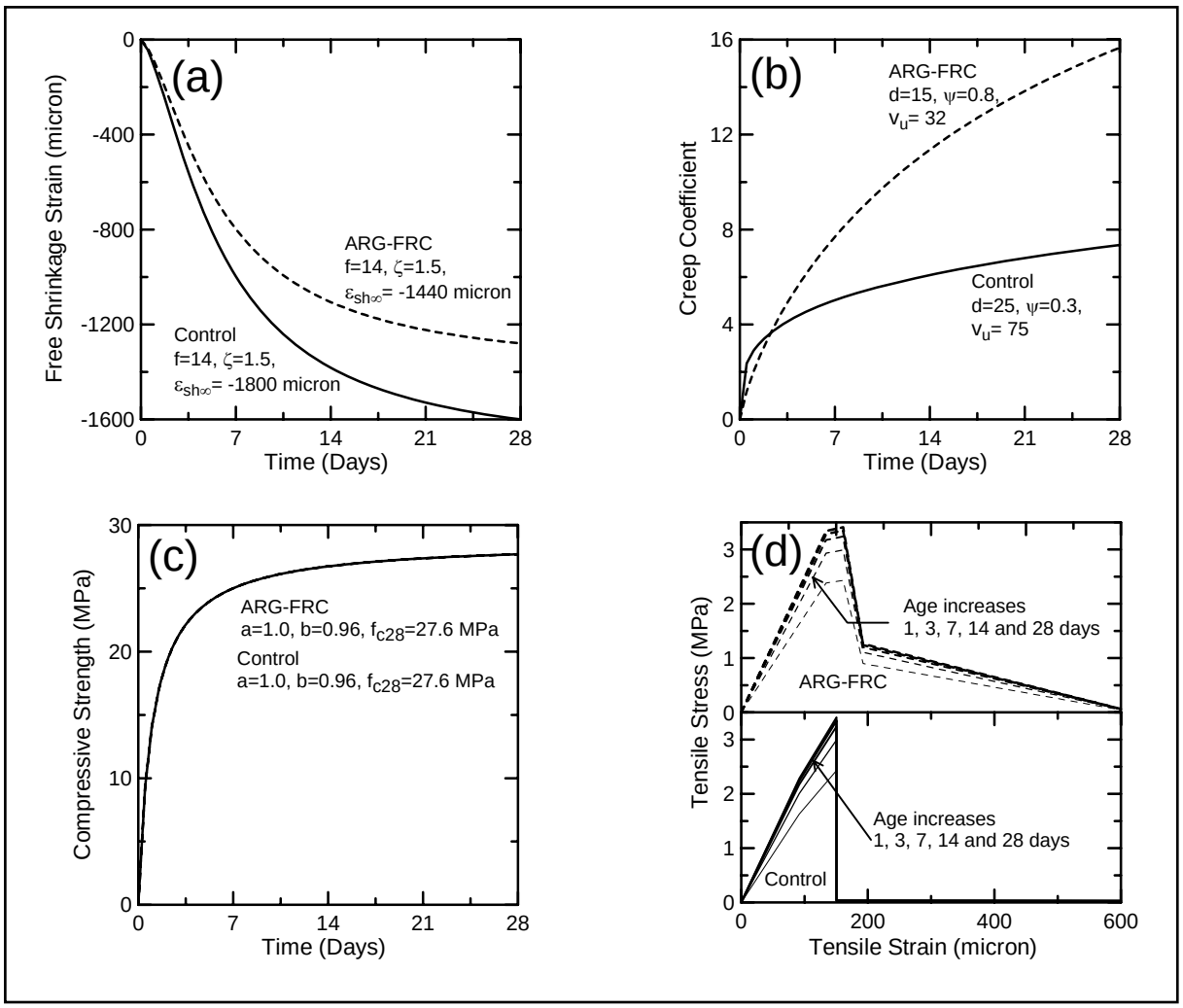

Fig. 6. Simulation input function for control and AR-GFRC mixes: (a) free shrinkage strain at outer concrete surface; (b) creep coefficient; (c) concrete compressive strength; (d) tensile stress–strain model

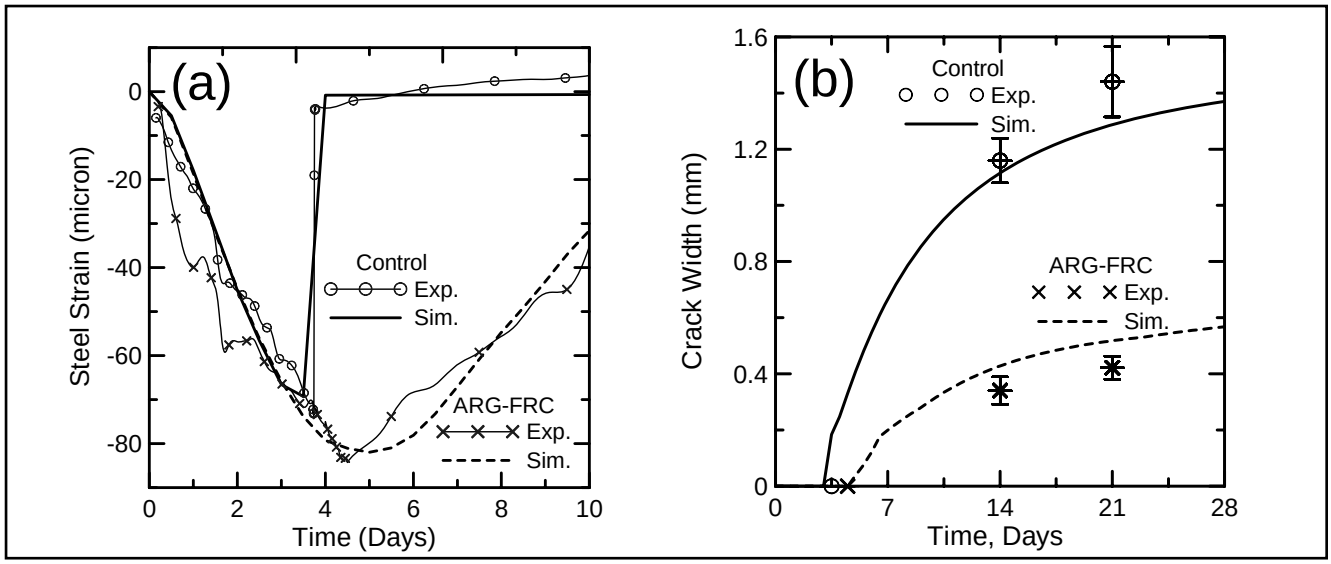

Fig. 7. Comparison between experimental result and model simulation: (a) strain history at steel ring; (b) crack width at outer concrete surface

5. Conclusions

The role of alkali-resistant (AR)-glassfibre in extending the crack resistance of concrete subjected to drying shrinkage is presented by experimental and analytical approaches. The results show that glassfibere can slightly delay the onset of cracking but drastically reduces crack width. With a small amount of glassfiber content, namely 3 kg/m^3 (5 lb/yd^3), the visible crack in the AR-GFRC occurred at 3.5 days as compared to 4.5 days in the control specimen, and after 21 days the crack width in the AR-GFRC specimen was only 0.3 times that of the control. The results are also supported by the developed model which was able to predict the shrinkage strains, shrinkage cracking, and crack width in plain and fiber-reinforced concrete.

6. Acknowledgement

The authors gratefully acknowledge the support of the National Science Foundation, Award No. 0324669-03, and Programme manager Dr P. Balaguru for his support of this research.

7. References

1. Grzybowski, M. and Shah, S.P. A model to predict cracking in fiber reinforced concrete due to restrained shrinkage. *ACI Materials Journal*, Vol. 87, No. 2, 1990, pp. 138–148.
2. American Association of State Highway and Transportation Officials. AASHTO Specification, *Standard Practice for Estimating the Cracking Tendency of Concrete*. AASTHO Designation: PP.34-99, 2005.
3. Weiss, J., Yang, W. and Shah, S.P. Influence of specimen size/geometry on shrinkage cracking of rings. *Journal of Engineering Mechanics, ASCE*, Vol. 126, No. 1, 2000, pp. 93–101.
4. Mane, S.A., Desai, T.K., Kingsbury, D. and Mobasher, B. *Modeling of Restrained Shrinkage Cracking in Concrete Materials*. SP-206, pp. 219–242.
5. Tuma, J.J. *Engineering Mathematics Handbook*. McGraw-Hill, 1970.
6. Bazant, Z.P. and Panula, L. Practical prediction of time-dependent deformation of concrete. Part 1: Shrinkage. Part 2: Creep. *Matériaux et Construction*, Vol. 11, No. 65, Sept.–Oct. 1978, pp. 307–328.
7. American Concrete Institute. ACI Committee 209. *Prediction of Creep, Shrinkage and Temperature Effects in Concrete Structures. Building Code Requirements for Reinforced Concrete*. ACI, Farmington Hills, 2002, ACI 209-92.